

See discussions, stats, and author profiles for this publication at: <https://www.researchgate.net/publication/227911668>

Electrochemical impedance spectroscopic study of titanium and its alloys in saline medium

ARTICLE *in* MATERIALS AND CORROSION · FEBRUARY 2007

Impact Factor: 1.37 · DOI: 10.1002/maco.200603979

CITATIONS

49

READS

46

3 AUTHORS:



Sengodan Tamilselvi

Anna University, Chennai

22 PUBLICATIONS 359 CITATIONS

SEE PROFILE



Murugaraj Rathinasamy

Anna University, Chennai

45 PUBLICATIONS 209 CITATIONS

SEE PROFILE



Rajendran Nallaiyan

Anna University, Chennai

134 PUBLICATIONS 1,323 CITATIONS

SEE PROFILE

Electrochemical impedance spectroscopic studies of titanium and its alloys in saline medium

S. Tamilselvi, R. Murugaraj and N. Rajendran*

The influence of potential on electrochemical behaviour of pure Ti, Ti-6Al-7Nb, and Ti-6Al-4V ELI alloy under saline conditions were investigated by electrochemical impedance spectroscopy (EIS). All measurements were carried out in saline solution (0.9% NaCl) at different impressed potentials (corrosion potential (E_{corr}), 0 mV (SCE) and + 500 mV (SCE)) for 1 h. The experimental results were compared with those obtained by potentiodynamic polarization curves. The corrosion current densities obtained for the

titanium alloys showed lower values than for pure Ti, indicating the formation of a stable passive film with time. Electrochemical impedance spectroscopic studies indicated that the resistance of the passive film increased with the impressed potential. The impedance spectra were fitted using a non-linear least square (NLLS) fitting procedure. The magnitude of the corrosion resistance of titanium alloys under saline solution was compared and results are presented.

1 Introduction

The most commonly used alloys for orthopaedic applications are type 316L stainless steel, Cr-Co alloys, Ti and its alloys. These alloys are primarily chosen as implants because of their biocompatibility and corrosion resistance, in addition to their structural properties such as high elastic modulus, yield strength and fracture toughness [1, 2]. Type 316L SS has been reported to show metallic wear and localized corrosion during long term contact with biological fluid [3].

Titanium and its alloys offer a unique combination of desirable mechanical properties, low density, high corrosion resistance and biocompatibility, which make them a more attractive material for structural and biomedical applications [4–6]. However, the conventional metallic biomaterials exhibit high corrosion resistance and the material degradation of a metal is never negligible [7, 8]. The corrosion process is determined by the ion release of metallic species and is, therefore, mainly a surface phenomenon. For titanium base alloys, the high titanium content promotes an easy reaction with oxygen from atmosphere due to its strong affinity for oxygen [9]. Thus, these materials show a tendency to form a stable and tightly adherent protective oxide layer on their surfaces. Solar et al. [10], have carried out the surface characterization of the passive film formed on Ti-6Al-4V surfaces in Ringer's solution. The passivity was observed over the potential range of – 400 to + 1400 mV vs SCE without breakdown. Further the pulse potentiostatic capacitance technique and Auger electron spectroscopy analysis of the specimens after the corrosion tests indicated that the electrochemical reaction occurring on the surface was the growth of a passive film. The Ti-6Al-7Nb alloy was developed [11] with mechanical properties comparable to those of high strength Ti-6Al-4V, but with better corrosion resistance [12]. In vitro studies have shown a

difference in cellular behaviour in the presence of debris generated by the wear of Ti-6Al-4V and Ti-6Al-7Nb alloys [13].

To determine the suitability of a material for body implant applications, several properties must be evaluated [14, 15]. Amongst these properties, the corrosion behaviour is of crucial interest; because of ion release from the implant to the surrounding tissues may give rise to biocompatibility problems. The objective of this work was to determine the corrosion behaviour of Ti, Ti-6Al-7Nb and Ti-6Al-4V ELI in saline (0.9% NaCl) solution at different impressed potentials (corrosion potential, 0 mV (SCE) and + 500 mV (SCE)) for 1 h. To achieve this objective, the different electrochemical techniques such as electrochemical impedance spectroscopy (EIS) and potentiodynamic polarization methods were used to study the corrosion behaviour of titanium alloys at different impressed potentials.

2 Experimental work

2.1 Sample preparation

Titanium, Ti-6Al-7Nb and Ti-6Al-4V ELI (TIMET, UK) samples of size 1 cm² were ground up to 1400 grit SiC paper, and the final polish was done using 6 and 1 microns alumina powder. The polished samples were ultrasonically cleaned with acetone, rinsed with deionized water, and dried. The 0.9% NaCl solution was used as electrolyte and the temperature was maintained at $37.4 \pm 1^\circ\text{C}$.

2.2 Electrochemical studies

2.2.1 Potentiodynamic polarization studies

Potentiodynamic polarization studies were carried out for titanium alloys in the saline solution. All the potential measurements were made with reference to a saturated calomel electrode (SCE). A platinum foil was used as the counter electrode. Polarisation measurements were carried out at a scan rate of 0.167 mV/s, in an aerated medium. A potentiostat (model PGSTAT 12, AUTOLAB, The Netherlands B.V) con-

* N. Rajendran, S. Tamilselvi, R. Murugaraj
Department of Applied Sciences and Humanities, MIT Campus,
Anna University,
Chromepet, Chennai-600 044 (India),
E-mail: nrjendran@annauniv.edu

trolled by a personnel computer with dedicated software (GPES version 4.9) was used for conducting the polarization experiments. In order to obtain reliable results, the polarization experiments were repeated three times in saline solution.

2.2.2 Electrochemical impedance spectroscopic (EIS) studies

Electrochemical Impedance Spectroscopy (EIS) studies were carried out at E_{corr} using an electrochemical system Frequency Response Analyser (FRA), which included a potentiostat model PGSTAT 12. The titanium specimen with the exposed surface of 1 cm^2 was used as the working electrode. The single sine wave measurements at frequencies between 10^4 Hz to 10^{-2} Hz were performed at different impressed potentials. Nyquist and Bode plots were obtained for the specimens immersed in the saline solution at the corrosion potential (E_{corr}), 0 mV (SCE), and $+500 \text{ mV}$ (SCE) for 1 h.

Electrochemical impedance spectroscopy uses very small amplitude signals that minimally perturb the electrodes [16–18]. Additionally, EIS provides the capabilities of studying corrosion reactions, measuring corrosion rates, estimation of the corrosion-resistance property of metals, determining and monitoring of multiple corrosion parameters that govern charge transfer and charge storage from the same measurement [19–21]. These include both faradaic processes (involving transfer of charge), such as metal ionization and formation of passive films, and non-faradaic processes (involving no transfer of charge), such as adsorption of species, reorientation of surface molecules, and diffusion effects.

Impedance spectra were represented in both complex impedance diagram (Nyquist plot) and bode amplitude and phase angle plots. In the Nyquist graph, the imaginary component ($-Z''$ ohm, out-of-phase) of impedance was plotted as a function of the real component (Z' ohm, in-phase), whereas the Bode representation shows the phase angle (θ) vs logarithm of the frequency f . The impedance spectra were modeled by fitting these data with an equivalent circuit. The software {EQUIVCRT} modeled by Boukamp was used in this study for EIS data modeling [22–23]. The impedance spectra were fitted using a non-linear least square (NLLS) fitting procedure. Because of the distributed relaxation feature, which is generally observed in titanium oxide films, a constant phase element (CPE) was utilized for data fitting instead of an ideal capacitor. The CPE considers the fact that experimentally, the oxide film never exhibits the theoretically expected phase shift of -90° and a slope of -1 for an ideal dielectric. Thus, a dissipation factor (n) is associated with them. This element is written in its admittance form as

$$Y^*(\omega) = Y_0(j\omega)^n \quad (1)$$

Where, Y_0 is the adjustable parameter used on the non-linear least-squares fitting, and n is defined as the phenomenological coefficient which can be obtained from the slope of $|Z|$ on the bode plot [22]. Pure capacitance is represented by $n = 1.0$. If n equals 0, then the CPE is a resistor. For example, a rough or porous surface can be modeled by a constant phase element with an n value between 0.9 to 1 [24], instead of a capacitance.

3 Results and discussion

3.1 Potentiodynamic polarisation measurements

The polarization test is a method of evaluating the corrosion property of metallic materials from the relation between the current density per unit surface area and the potential scanned artificially. The current density directly indicates the dissolution of metallic ions from the materials into the electrolyte, namely the state of corrosion.

Figs. 1–3 show the cathodic and anodic polarization curves for pure Ti, Ti-6Al-7Nb and Ti-6Al-4V ELI implant alloys respectively in saline solution at different impressed potentials for a period of one hour. The corrosion current density (i_{corr}) and corrosion potential (E_{corr}), observed for pure Ti, Ti-6Al-7Nb and Ti-6Al-4V ELI are given in the Table 1. The corrosion potential (E_{corr}) values obtained for Ti, Ti-6Al-7Nb and Ti-6Al-4V ELI at impressed potential of $+500 \text{ mV}$ were -220 mV , -202 mV and -304 mV respec-

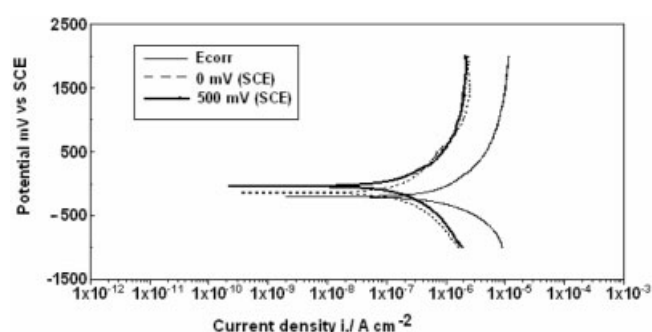


Fig. 1. Potentiodynamic polarization curves of pure Ti at different impressed potentials in saline solution

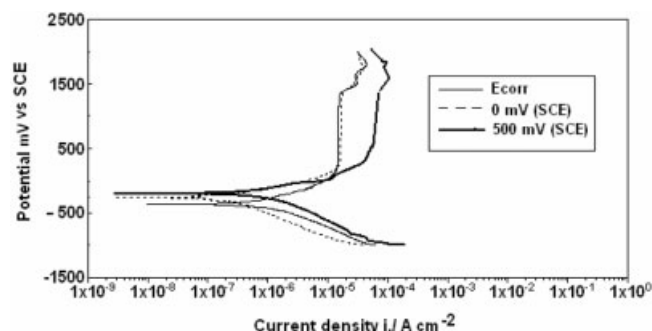


Fig. 2. Potentiodynamic polarization curves of Ti-6Al-7Nb alloy at different impressed potentials in saline solution

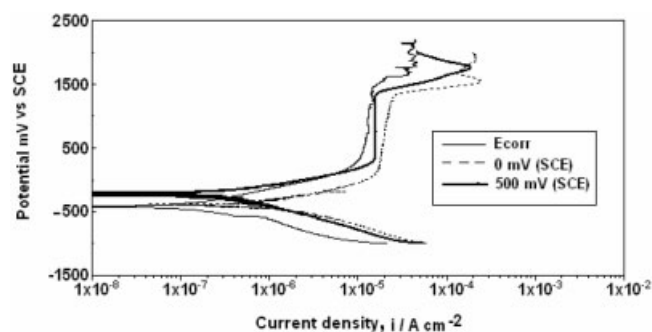


Fig. 3. Potentiodynamic polarization curves of Ti-6Al-4V ELI alloy at different impressed potentials in saline solution

Table 1. Potentiodynamic polarization curves of Ti, Ti-6Al-7Nb and Ti-6Al-4V ELI at different impressed potentials in saline solution

Potential mV vs SCE	Ti		Ti-6Al-7Nb		Ti-6Al-4V ELI	
	E_{corr} [mV] vs SCE	I_{corr} [A cm^{-2}]	E_{corr} [mV] vs SCE	I_{corr} [A cm^{-2}]	E_{corr} [mV] vs SCE	I_{corr} [A cm^{-2}]
E_{corr}	– 387	5.97×10^{-7}	– 361	6.80×10^{-7}	– 401	4.84×10^{-7}
0	– 294	7.12×10^{-7}	– 256	7.25×10^{-7}	– 395	6.05×10^{-7}
500	– 220	3.05×10^{-8}	– 202	9.58×10^{-8}	– 304	1.06×10^{-8}

tively. It is observed from the figures that I_{corr} decreases and E_{corr} increases for all the samples impressed at 500 mV for 1 h. These results indicate that the corrosion resistance of titanium alloys in saline solution was found to be satisfactory. The corrosion density (I_{corr}) values obtained for Ti, Ti-6Al-7Nb and Ti-6Al-4V ELI were $3.05 \times 10^{-8} \text{ A cm}^{-2}$, $9.58 \times 10^{-8} \text{ A cm}^{-2}$ and $1.06 \times 10^{-8} \text{ A cm}^{-2}$ respectively at impressed potential of + 500 mV in saline solution. In the literature, it has been reported that the corrosion current density of Ti-6Al-4V implant alloy is as high as $45.93 \mu\text{A cm}^{-2}$ in 0.6 M NaCl solution at room temperature [25], $38.48 \mu\text{A cm}^{-2}$ in 25 wt% H_2SO_4 solution, $13.35 \mu\text{A cm}^{-2}$ in 7.5 wt% HCl solution [26].

From Fig. 2, the increase in impressed potential from E_{corr} to + 500 mV, an increase in the thickness of the passive oxide film was observed and also exhibited higher corrosion resistance for alloy Ti-6Al-7Nb compared to Ti-6Al-4V ELI, due to the following reasons. Titanium and its alloys generally possess a spontaneously formed oxide film on the surface as TiO_2 , and small amounts of Ti_2O_3 , Al, V or Nb oxides. Increased corrosion stability of the Ti-6Al-7Nb was observed due to

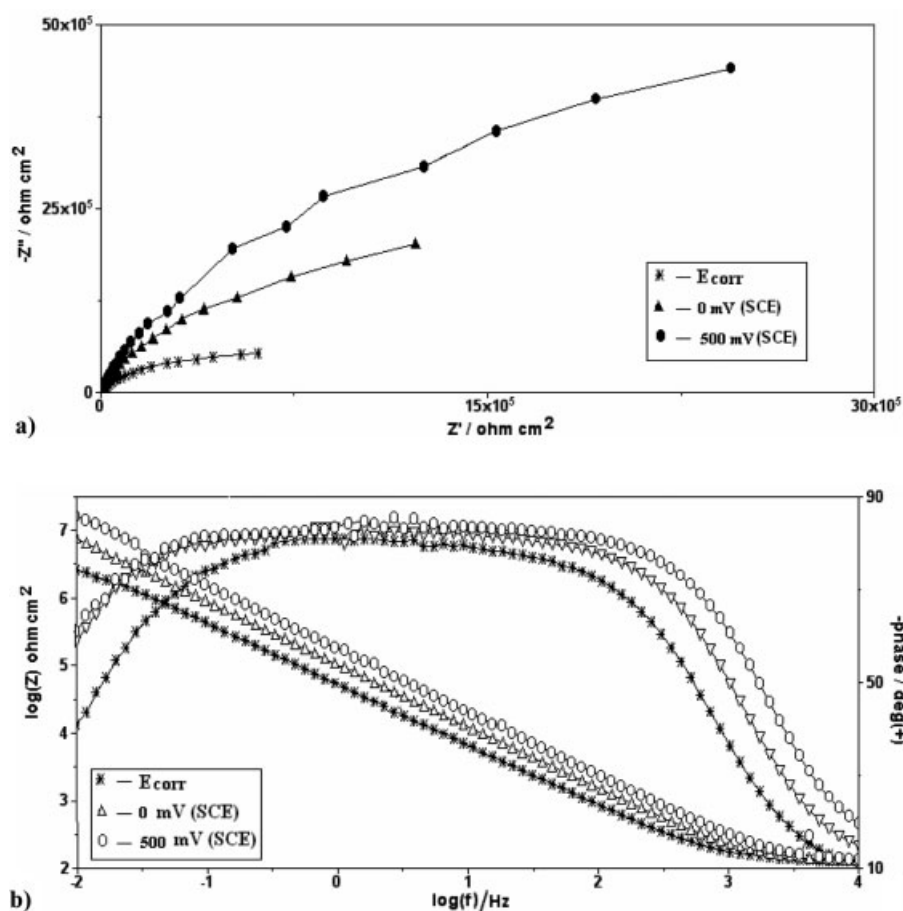
the beneficial effect of the Nb(V) oxide on the titanium passive oxide film whereas for Ti-6Al-4V ELI, localized corrosion occur due to the dissolution of vanadium at the surface film/electrolyte interface [27].

The Ti-6Al-7Nb alloy showed superior corrosion resistance than the Ti-6Al-4V ELI alloy in the polarization test in 0.9% NaCl solution. It was believed that the Ti-6Al-7Nb alloy attains more corrosion resistance in the physiological environments for use as orthopaedic devices.

3.2 Electrochemical impedance spectroscopy

3.2.1. Impedance results of the Ti and Ti-6Al-7Nb alloys in saline solution

Electrochemical impedance experiments performed at different impressed potentials viz., at corrosion potential (E_{corr}), 0 mV (SCE) and + 500 mV (SCE) for 1 h are shown in Figs. 4–6. The properties of the passive layers on the Ti

**Fig. 4(a).** Nyquist plots of pure Ti at different impressed potentials in saline solution**Fig. 4(b).** Bode plots of pure Ti at different impressed potentials in saline solution

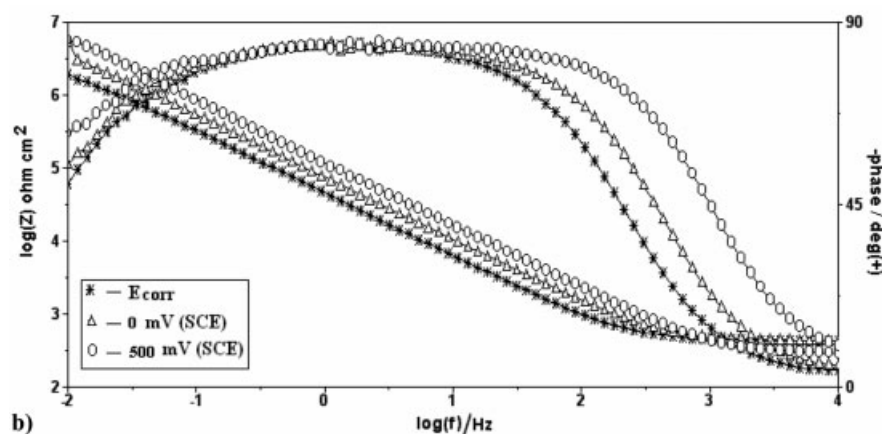
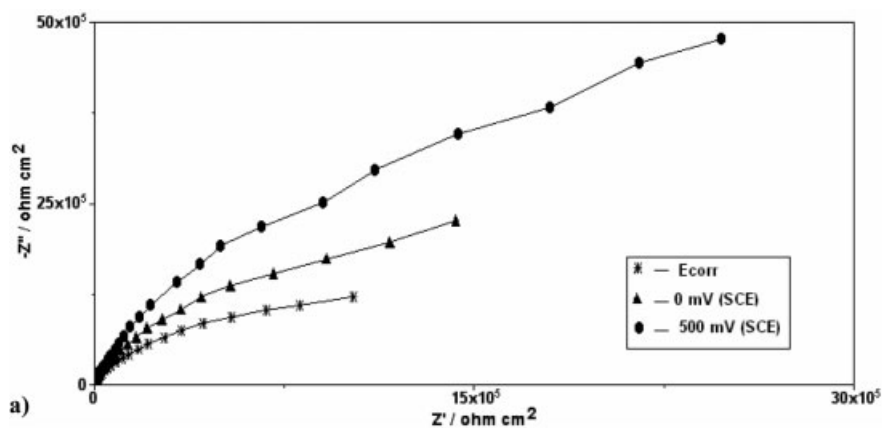


Fig. 5(a). Nyquist plots of Ti-6Al-7Nb alloy at different impressed potentials in saline solution

Fig. 5(b). Bode plots of Ti-6Al-7Nb alloy at different impressed potentials in saline solution

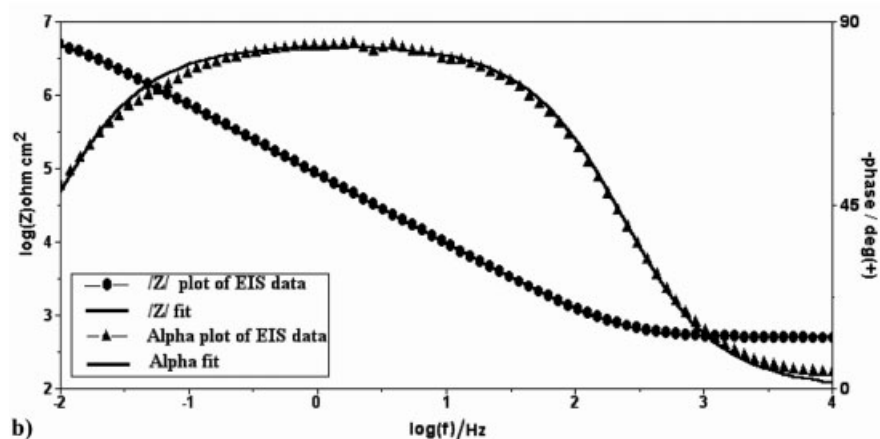
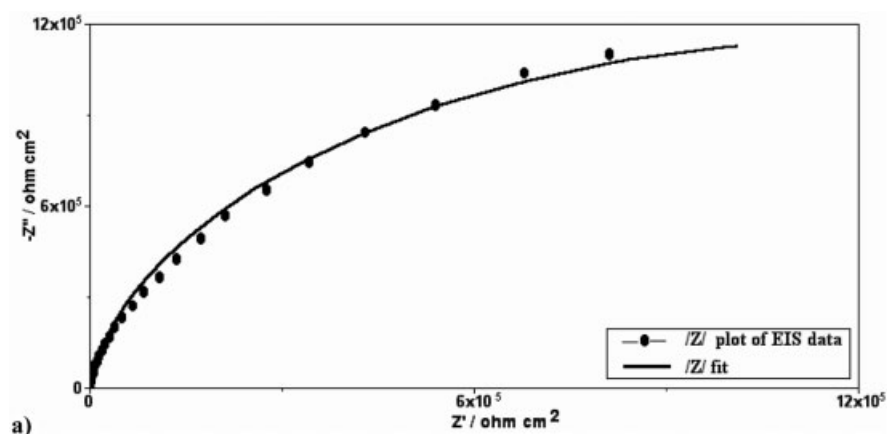
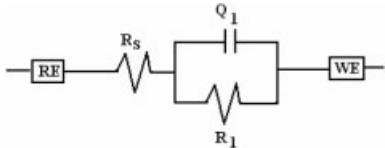


Fig. 6(a). Nyquist plot of Ti-6Al-7Nb alloy in the saline solution. The symbol (—●—) represents measured data, the full line (—) represents fitted values based on the NLLS analysis

Fig. 6(b). Bode plot of Ti-6Al-7Nb alloy in the saline solution. The symbols (—●— —▲—) represent measured data, the full line (—) represents fitted values based on the NLLS analysis

Table 2. Values of fitting parameters obtained by fitting the $R_s(Q_1R_1)$ model to the EIS data as a function of impressed potential in saline solution for Ti and Ti-6Al-7Nb


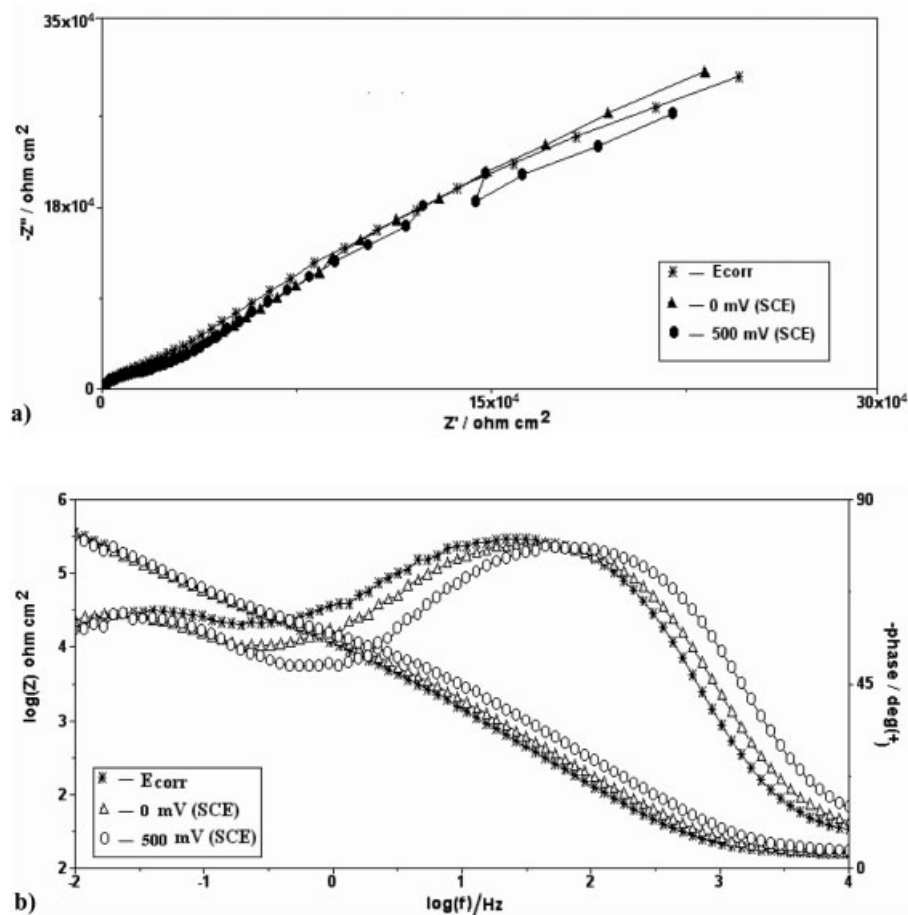
Materials	Impressed potential [mV] vs SCE	R_s [ohm cm^2]	Q_1 $\mu\text{F cm}^{-2}$	n	R_1 [Mohm cm^2]
Titanium	E_{corr}	11.088	11.712	0.9039	0.3315
	0	10.976	7.2428	0.9236	1.5596
	500	11.256	0.3875	0.9402	3.2844
Ti-6Al-7Nb	E_{corr}	42.924	11.2321	0.9406	0.7101
	0	44.828	6.2392	0.9408	1.5988
	500	28.924	0.2998	0.9448	3.4720

and Ti-6Al-7Nb alloys were compared using EIS techniques. They are displayed in both complex impedance (Nyquist diagram) and Bode amplitude and phase angle plots.

Fig. 4(b) and Fig. 5(b) show the Bode plot for Ti and Ti-6Al-7Nb alloy at different impressed potentials in saline solution. It was observed from the figures that the impedance was constant between the frequency ranges of 10^{-2} – 10^2 Hz, indicating a compact passive oxide film on the titanium alloy. The phase angle maximum (θ max) observed for Ti and Ti-6Al-7Nb alloy was found to lie in the range

of approximately -80° to -86° . The values of the phase angle maximum, which span four frequency decades (0.1 Hz to 100 Hz), gradually decreases with decreasing frequency (below 0.1 Hz). It is thought that the stable passive film on titanium alloys behaves as an efficient barrier to corrosion, and increases the resistance to charge transfer at the corrosion interface.

For the interpretation of the electrochemical behaviour of a system from EIS spectra, an appropriate physical model of the electrochemical reactions occurring on the electrode is neces-

**Fig. 7(a).** Nyquist plots of Ti-6Al-4V ELI alloy at different impressed potentials in saline solution**Fig. 7(b).** Bode plots of Ti-6Al-4V ELI alloy at different impressed potentials in saline solution

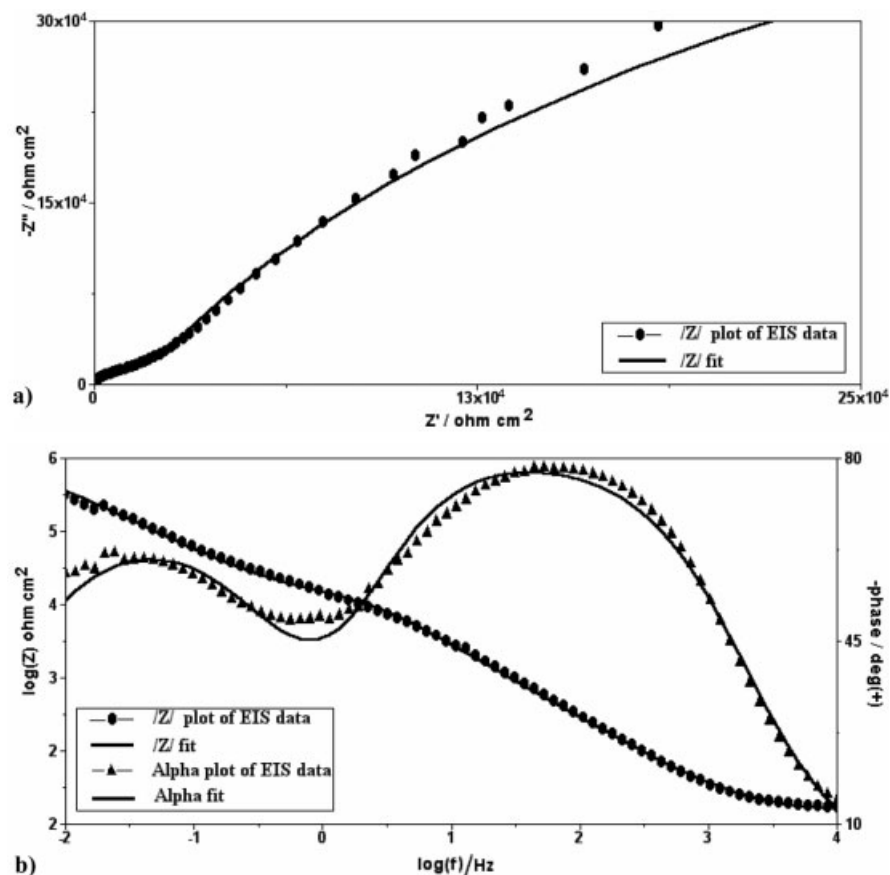


Fig. 8(a). Nyquist plot of Ti-6Al-4V ELI alloy in the saline solution. The symbol (●) represents measured data, the full line (—) represents fitted values based on the NLLS analysis.

Fig. 8(b). Bode plot of Ti-6Al-4V ELI alloy in the saline solution. The symbols represent (●) measured data, the full line (—) represents fitted values based on the NLLS analysis.

sary [28]. In titanium and Ti-6Al-7Nb alloy, the EIS curves obtained are dependant on impressed potentials. The equivalent circuits used to represent these diagrams are presented in Table 2 and in Fig. 6(a) and (b). The circuit description code (CDC) is $R_s(R_1Q_1)$. The equivalent circuit consists of R_1 (charge transfer resistance (R_{ct})) which is in parallel with a Q_1 (double layer capacitance (C_{dl})), and both of these elements are in series with the solution resistance (R_s). From the table, R_s is the total ohmic or solution resistance of the electrochemical cell and contains contributions from the solution, cables and other sources. R_1 is considered to be the corrosion resistance of the alloy, which is inversely proportional to the corrosion current density. It is also observed that the R_1 values increase as increasing the potential for titanium and Ti-6Al-7Nb alloy whereas Q_1 values decrease with increasing the impressed potential and also the n values were approximately equal to 1, which indicates an ideal capacitor.

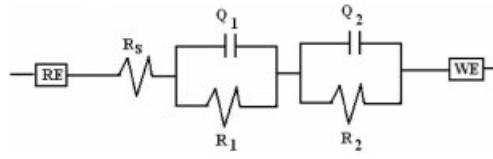
3.2.2. Impedance results of the Ti-6Al-4V ELI alloys in saline solution

Fig. 7(a) and (b) show the Nyquist and Bode plot of Ti-6Al-4V ELI alloy in saline solution at different impressed potentials (E_{corr} 0 mV (SCE) and + 500 mV (SCE)). The Bode plot exhibits two time constants at all impressed potentials, as evidenced by the appearance of two distinct frequency regions. The time constant in the high-frequency part arises from the uncompensated ohmic resistance due to the electrolytic solution. However, at the low frequency part, the phase angle θ decreased almost linearly to a constant value of approximately

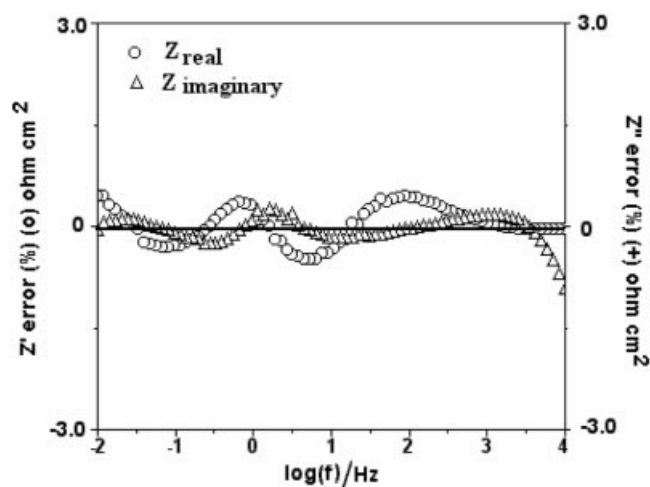
– 50°, suggesting the occurrence of the diffusion process in the solid phase at the substrate/electrolyte interface. The diffusion process may be due to the dissolution of vanadium oxide. This oxide is readily soluble and reacts with Cl^- ions in aqueous media [27, 29]. These processes are further accelerated by the presence of chloride ions in physiological solution. As the consequence of adsorption of the Cl^- ions, the stability of the oxide layer decreases and the localized corrosion susceptibility of the Ti-6Al-4V ELI alloy increases. Similar results were also reported in the literature [30].

The equivalent circuits used to represent these diagrams are presented in the Table 3. Fig. 8(a) and (b) show the well fitted Nyquist and Bode plot for Ti-6Al-4V ELI in saline solution. The circuit description code (CDC) is $R_s(R_1Q_1)(R_2Q_2)$. The equivalent circuit consists of solution resistance (R_s), double layer capacitances (Q_1 , Q_2) and charge transfer resistance (R_1 , R_2) respectively. It is evinced that the elements represented in both circuits as capacitors Q_1 and Q_2 were fitted as constant phase elements. This is general diffusion related to element Q which accounts for deviation from ideal dielectric behaviour related to surface/bulk inhomogeneties or current leakage in the interface/electrolyte [31].

Fig. 9 shows the error distribution (E %) for Ti-6Al-4V ELI alloy in saline solution. A reasonable fit to the equivalent circuit for a given impedance spectra was established by admitting a relative error of less than 1% for the real and imaginary parts of the impedance [22]. Next, the quality of fitting was judged by the error distribution vs the frequency comparing experimental with simulated data for different models. From the figure, it is observed that less than 1% showed perfect fitting for the Ti-6Al-4V ELI alloy in saline solution.

Table 3. Values of fitting parameters obtained by fitting the $R_s(Q_1R_1)(Q_2R_2)$ model to the EIS data as a function of impressed potential in saline solution for Ti-6Al-4V ELI


Material	Impressed potential mV vs SCE	R_s [ohm cm ²]	Q_1 [μF cm ⁻²]	n_1	R_1 [Mohm cm ²]	Q_2 [μF cm ⁻²]	n_2	R_2 [Mohm cm ²]
Ti-6Al-4V ELI	E_{corr}	13.496	27.1857	0.9537	5.1072	16.7482	0.8712	0.2923
	0	12.852	15.6071	0.9591	5.6588	12.8285	0.8497	0.3497
	500	12.824	11.5714	0.9623	5.6661	5.2464	0.8039	0.3340

**Fig. 9.** Fit errors of Z_{real} and $Z_{imaginary}$ of Ti-6Al-4V ELI alloy in saline solution

4 Conclusions

Based on the polarisation and impedance spectroscopic measurements, the following conclusions can be drawn:

The corrosion current density decreases and the corrosion potential increases with increasing the impressed potentials. Ti-6Al-7Nb alloy showed a much better corrosion resistance than Ti-6Al-4V ELI alloy in saline solution due to its high content of niobium and aluminum, which promoted repassivation. The order of the corrosion resistance under saline solution is Ti-6Al-7Nb > Ti > Ti-6Al-4V ELI. The ac circuit elements for the corrosion interface of Ti and its alloys in saline solution were calculated based on the equivalent circuit model. Theoretical model predictions are in good agreement with the experimental results. The n values for Ti, Ti-6Al-4V ELI and Ti-6Al-7Nb were found to be 0.90, 0.87 and 0.94 respectively at E_{corr} . Similar n values were observed for all the alloys at 0 and 500 mV impressed potentials. Hence, the n values for Ti-6Al-7Nb are nearer to 1, which behaves as an ideal capacitor.

5 References

- [1] D. F. Williams, *Mater. Sci.* **1987**, 22, 3421.
- [2] H. Zitter, H. Plank Jr., *J. Biomed. Mater. Res.* **1987**, 21, 881.
- [3] D. F. Williams (Ed.), *Medical and Dental Materials Materials Science and Technology, A Comprehensive Treatment*, R.W. Cahn, P. Hassen, E. J. Kramer (Eds), Vol. 14, VCH, Weinheim, **1992**.
- [4] A. Shenhar, I. Gotman, *Mater. Sci. Eng. A* **1991**, 268, 40.
- [5] H. Sibum, V. Guthier, O. Roidl, in: *Alloys – Preparation, Properties, Applications*, F. Habashi (Ed.), (ch.11) Wiley, VCH, Weinheim, **1998**.
- [6] R. Strietzel, A. Hoseh, H. Kalbfleisch, D. Buch, *Biomaterials* **1998**, 19, 1945.
- [7] H. J. Breme, V. Biehl, J. A. Helsen, in: J. A. Helsen, H. J. Breme (Eds.), *Metals as Biomaterials* (Ch.2), Wiley, Chichester, **1998**.
- [8] D. H. Kohn, P. Ducheyne, in: D. F. Williams (Ed.), *Medical and Dental Materials, Materials Science and Technology*, Vol.14 (Ch.2) VCH Weinheim, **1992**.
- [9] M. F. Lopez, A. Gutierrez, J. A. Jimenez, *Surf. Sci.* **2001**, 300, 482.
- [10] R. I. Solar, S. R. Pollack, E. Korostoff, *J. Biomed. Mater. Res.* **1979**, 13, 217.
- [11] M. F. Semlitsch, H. Weber, R. M. Streicher, R. Schon, *Biomaterials* **1992**, 13, 781.
- [12] E. Kobayashi, T. J. Wang, H. Doi, T. Yoneyama, H. Hamanaka, *Mater. Sci. Mater. Med.* **1998**, 9, 567.
- [13] D. Rugers, D. W. Howie, S. E. Graves, M. J. Pearcy, D. R. Haynes, *J. Bone Joint Surg* **1997**, 79B, 311.
- [14] M. Niinomi, D. Kuroda, K. Fukunaga, M. Morinaga, Y. Kato, T. Yashiro, A. Suzuki, *Mater. Sci. Eng. A* **1999**, 263, 193.
- [15] S. Tamilselvi, V. Raman, N. Rajendran, *Proceedings of the International Convention of Surface Engineering*, INCO-SURF, 25–27 August, **2004**, 487.
- [16] F. Mansfeld, *Corrosion* **1981**, 36, 301.
- [17] EG&G Princeton Applied Research, Princeton, N.J Application Note AC-1, **1985**, *Basic of electrochemical impedance spectroscopy (EIS)*.
- [18] W. S. Tait, *An Introduction to Electrochemical Corrosion Testing for Practicing Engineers and Scientists*, Pair O Docs Publications, Racine, WI, **1994**, pp. 79 and 95.
- [19] H. Xiao, F. Mansfeld, *J. Electrochem. Soc.* **1994**, 141, 2332.
- [20] A. S. M. Rautenbach, P. C. Pistorius, J. E. Leitch, *Poly. Mater. Sci. Eng.* **1996**, 740, 14.
- [21] F. Mansfeld, *Corrosion* **1996**, 52, 417.
- [22] B. A. Boukamp, *Equivalent circuits, Manual AC immittance data analysis system*, Enschede, University of Twente, The Netherlands **1989**.
- [23] B. A. Boukamp, *Solid State Ionics* **1986**, 21, 31.

- [24] R. M. Souto, M. M. Laz, R. L. Reis, *Biomaterials* **2003**, 24, 4213.
- [25] S. K. Yen, T. Y. Huang, *Mater. Chem. Phys.* **1998**, 56, 214.
- [26] L. Gokulakshami, D. Arivuoli, B. Ganguli, *Mater. Chem. Phys.* **2002**, 76, 187.
- [27] I. Milosev, M. Metikos-Hokovic, H. Strenblow, *Biomaterials* **2000**, 21, 2103.
- [28] A. J. Bard, L. R. Faulkner, *Electrochemical methods: Fundamentals and applications*, 2nd ed., New York, Wiley **2001** (Chapter 10).
- [29] M. Ask, J. Lausmaa, B. Kasemo, *Appl. Surf. Sci.* **1988–89**, 35, 283.
- [30] M. Metikos-Hukovic, A. Kwokal, J. Piljac, *Biomaterials* **2003**, 24, 3765.
- [31] C. Fonseca, M. A. Barbosa, *Corros. Sci.* **2001**, 43, 547.

(Received: March 3, 2006)

W 3979